catalysts

MDPI

Communication

Residual Trifluorosulfonic Acid in Amino-Functionalized Covalent Triazine Frameworks for Boosting Photocatalytic Hydrogen Evolution

Chengxiao Zhao [1,*], Zhaolin Li [1,2] and Weiping Xiao [1,*]

[1] College of Science, Nanjing Forestry University, Nanjing 210037, China; zhaolinli@njfu.edu.cn
[2] School of Chemistry and Chemical Engineering, Southeast University, Nanjing 211189, China
* Correspondence: chengxiaozhao@njfu.edu.cn (C.Z.); wpxiao@njfu.edu.cn (W.X.)

Abstract: The utilization of covalent triazine frameworks (CTFs) as photocatalysts has witnessed rapid advancements in the field of photocatalysis. However, the presence of residual components in certain CTFs materials is widely ignored as regards their influence on photocatalytic performance. In this study, we find that trifluorosulfonic acid (TfOH) molecules stably exist in the amino-functionalized CTF-NH_2 framework, which enhance the affinity for water. The experimental results indicate that the residual TfOH elevates the VB position of CTF-NH_2, facilitating the oxidization of both water and sacrificial agents. Moreover, the present of TfOH accelerates the separation and transfer of photogenerated charge carriers to the Pt cocatalyst. Consequently, CTF-NH_2-F containing residual TfOH molecules demonstrates a significant enhancement in the photocatalytic hydrogen evolution, achieving about 250 μmol over a duration of 3 h of illumination, which represents a 2.5-fold increase compared to that observed for CTF-NH_2. This research underscores the substantial impact that residues exert on photocatalytic performance.

Keywords: photocatalysis; photocatalytic hydrogen production; covalent organic frameworks; covalent triazine frameworks; amino functionalization

Academic Editor: Jorge Bedia

Received: 15 November 2024
Revised: 21 December 2024
Accepted: 24 December 2024
Published: 26 December 2024

Citation: Zhao, C.; Li, Z.; Xiao, W. Residual Trifluorosulfonic Acid in Amino-Functionalized Covalent Triazine Frameworks for Boosting Photocatalytic Hydrogen Evolution. *Catalysts* **2025**, *15*, 12. https://doi.org/10.3390/catal15010012

1. Introduction

The advancement of photocatalytic hydrogen production from water is of significant importance in addressing the growing demand for renewable energy. A variety of photocatalysts for water splitting into hydrogen have been systematically developed [1–4]. Nitrogen-rich covalent organic frameworks (COFs), distinguished by their remarkable chemical and physical stability and high crystallinity, as well as heteroatomic effect, have garnered significant attention [5–7]. The intriguing observation is that COFs with identical structures generated through different methodologies may exhibit varying levels of photocatalytic activity. The prevailing consensus among researchers is that the variation in synthesis methods primary leads to changes in the microstructures and surface defects of COFs, subsequently inducing the differences in electronic properties and active sites [8–10]. It is important to acknowledge that the utilization of certain specific synthesis methods for COFs inevitably results in the retention of particular components, an aspect that often goes unrecognized in its influence on photocatalytic activity.

Researchers have discovered that some dopants can alter charge carrier dynamics or introduce additional pathways for photogenerated electron-hole separation—factors crucially affecting overall catalytic efficiency [11–13]. For example, during the synthesis of zinc hydroxystannate, a trace amount of SnO_2 could form on its surface, acting as

photoactive sites that facilitate the generation of charge carriers to realize the photocatalytic degradation of gaseous benzene by zinc hydroxystannate [14]. The incorporation of single atom Ag (Ag/TiO_2 = 0.5 wt.%) into TiO_2@PF3T results in the formation of Ag bonding between PF3T nanocluster and TiO_2, enabling ultra-stable visible light driven photocatalytic H_2 production [13]. Additionally, photocatalysts synthesized through metal-catalyzed coupling reactions typically contain trace metal impurities [15]. A recent study on C(sp^3)-H functionalization revealed that residual trace Fe exhibits significantly catalytic activity [16]. Likewise, specific trace anions can also improve the photocatalytic activity in specific photocatalytic systems. In the case of the acridinium perchlorate-based photocatalysts, trace chloride anions derived from acridinium perchlorate salts exhibit hydrogen atom transfer catalysis capabilities, facilitating the efficient activation of primary C(sp^3)-H bonds [17]. The above research studies demonstrate that the residual components within the COFs may exert a significantly influence on their photocatalytic performance.

Covalent triazine frameworks (CTFs) with a nitrogen-rich architecture have emerged as one of the highly promising organic porous photocatalysts for hydrogen production [18,19]. Especially of note, CTFs featuring an alternating structure of triazine and phenylene exhibit high photocatalytic performance and can be synthesized using low-cost precursors through a straightforward acid-catalyzed polymerization process [20,21]. Nevertheless, acid molecules are inevitably present in CTFs, which is often disregarded in studies focusing on photocatalysis [22]. Here, we find that trifluorosulfonic acid (TfOH) molecules exhibit enhanced affinity towards the amino-functionalized CTF-NH_2. Our study reveals that residual TfOH not only increases the VB position of CTF-NH_2-F, facilitating water oxidization or consumption of photogenerated holes, but also accelerates the separation and transfer of photogenerated charge carriers to the Pt cocatalyst. As a result, a pronounced enhancement in the photocatalytic hydrogen evolution was observed for CTF-NH_2-F. The photocatalytic hydrogen evolution of CTF-NH_2-F reached about 250 μmol in 3 h, exhibiting a 2.5-fold increase compared to that of CTF-NH_2.

2. Results and Discussion

2.1. Preparation of Samples

The photocatalysts CTF-1, CTF-NH_2 and CTF-NH_2-F (Figure S1) were synthesized according to the methodology described in our previous research [23]. The only distinction lies in the treatment of the resulting polymerized covalent framework, where ammonia is employed to obtain CTF-NH_2 and CTF-1, while non-ammonia treatment yields CTF-NH_2-F and CTF-1-F. FTIR, XPS and XRD analyses were carried out to verify the structure of CTF-NH_2-F. In the FTIR spectra (Figure 1a), the vibration peaks observed at 1516 cm^{-1}, 1356 cm^{-1}, and 813 cm^{-1} were assigned to the triazine moiety [24,25]. In comparison to CTF-NH_2, two new peaks appeared at wavenumbers of 1170 cm^{-1} and 1034 cm^{-1}, which were ascribed to the asymmetric and symmetric stretching vibrations of C-F and S=O in trifluorosulfonic acid (TfOH) [26,27]. In the XPS spectrum of CTF-NH_2-F (Figure 1b,c and Figure S2), both F and S elements were identified, and the distinct peaks corresponding to C=N, -NH_2 and S=O were successfully fitted. These results indicate that a number of residual TfOH molecules persist in CTF-NH_2-F.

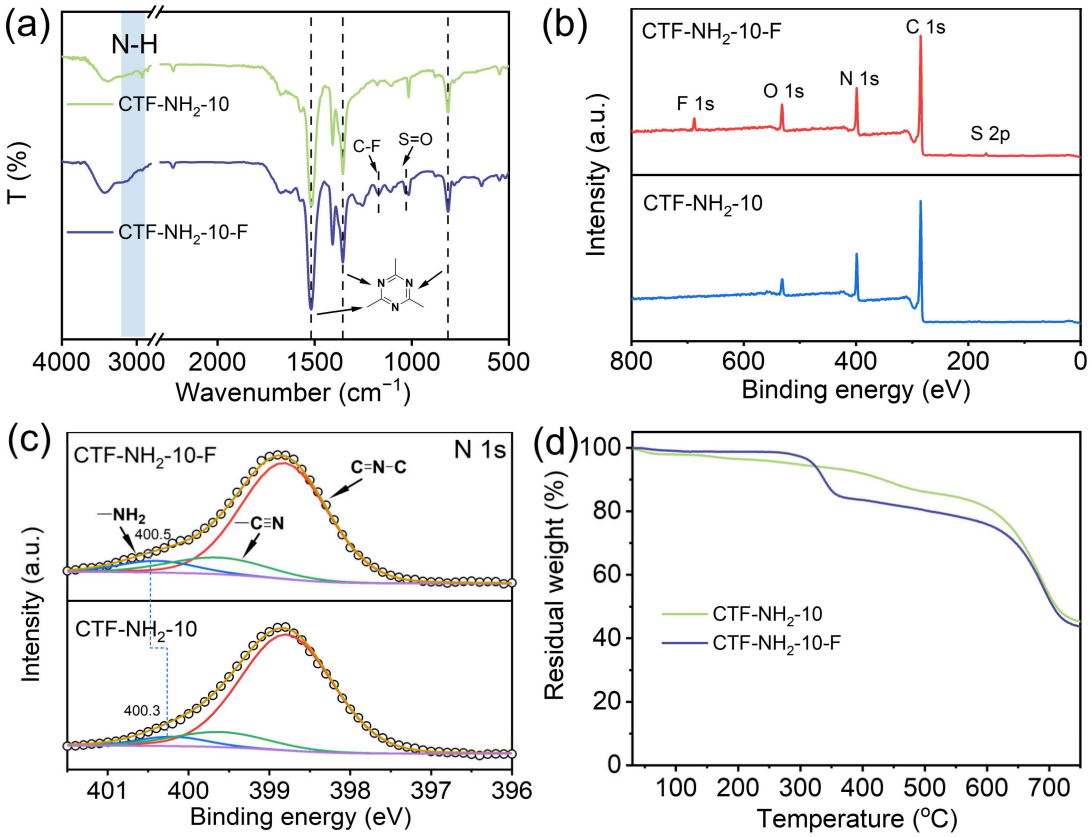

Figure 1. (**a**) FT-IR spectra, (**b**) XPS survey spectra, (**c**) high-resolution N 1s XPS spectra and (**d**) TG spectra of CTF-NH_2-10 and CTF-NH_2-10-F.

Elemental analysis indicates that the sulfur content in CTF-NH_2-10-F is about 1.24 wt.%, which corresponds to a TfOH content of 5.8 wt.% (Table S1). The TG curve of CTF-NH_2 shows a gradual mass reduction of ca. 7 wt.% as the temperature rises below 400 °C (Figure 1d). In contrast, CTF-NH_2-F exhibits a mass loss of about 15 wt.% at 340 °C, which is 8 wt.% higher than that of CTF-NH_2. This observation suggests the release of residual TfOH and adsorption water at high temperature, which underscores the stable existence of TfOH molecules in CTF-NH_2-F. Nevertheless, the residual TfOH molecules did not affect the crystal structure and morphology of the frameworks, as evidenced by the similar XRD patterns and SEM images of CTF-NH_2-F and CTF-NH_2 (Figure 2a–d and Figure S3).

2.2. Photocatalytic Hydrogen Evolution

The obtained samples of CTF-NH_2-F containing residual TfOH were initially subjected to the measurement of photocatalytic hydrogen evolution. Compared to the pure CTF-NH_2, a significant enhancement in hydrogen evolution was observed for CTF-NH_2-F (Figure 3a,b, Figures S4 and S5). Especially of note, CTF-NH_2-10-F showed a hydrogen production rate of 4.5 mmol g^{-1} h^{-1}, representing an improvement of about 2.5-fold compared to that of CTF-NH_2-10. Moreover, the AQYs at 420 nm, 450 nm and 520 nm were measured as 3.56%, 2.59% and 0.3% for CTF-NH_2-10-F (Figure 3c), respectively [28]. Additionally, the photocatalytic stability of CTF-NH_2-10-F was slightly reduced, which was evidenced by the cycle test (Figure 3d). Additionally, the photocatalytic hydrogen evolution of pure CTF-1 and CTF-1-F untreated with ammonia were also evaluated, and they exhibited similar yet markedly low photocatalytic performance (Figure 3b). These results indicate that the performance improvement of CTF-NH_2-F may primarily originate from the interaction between residual TfOH and amino groups.

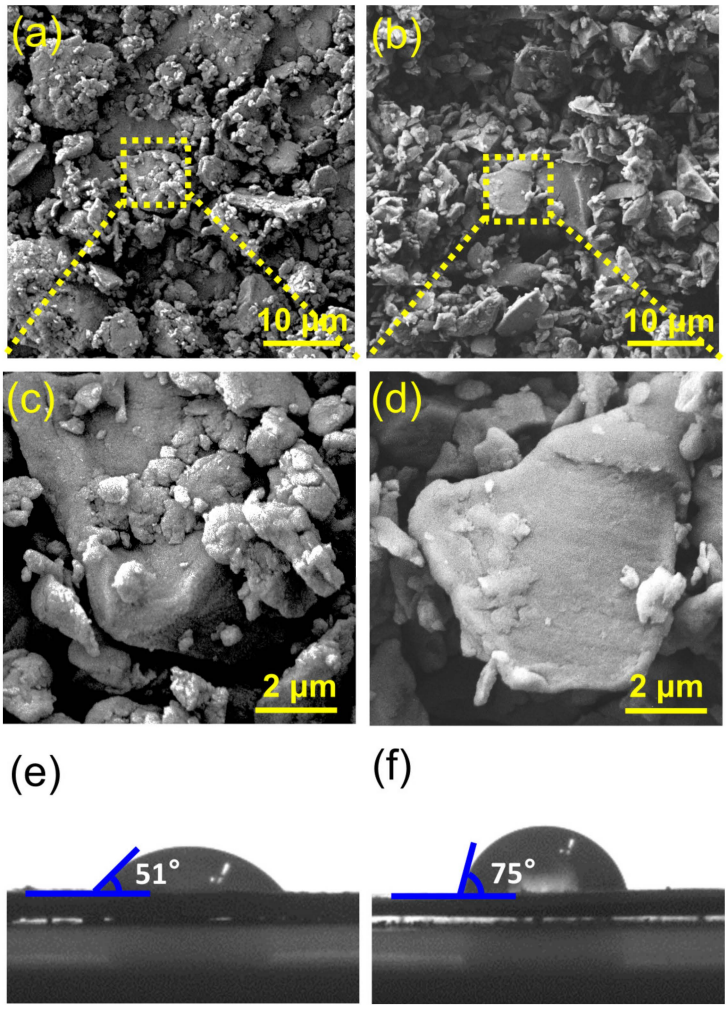

Figure 2. SEM images and water contact angles of (**a**,**c**,**e**) CTF-NH_2-10-F and (**b**,**d**,**f**) CTF-NH_2-10.

In order to elucidate the improvement in hydrogen production for CTF-NH_2-F, a comparison of the FTIR spectra for CTF-NH_2 and CTF-NH_2-F was performed (Figure 1a), revealing a slight increase in intensity within the wavenumber range of 3110–3220 cm^{-1} for CTF-NH_2-F, indicative of the associated N-H bonds. Correspondingly, the binding energy assigned to -NH_2 (400.3 eV) exhibited a shift towards higher energy in the high-resolution N 1s spectrum (Figure 1c). Additionally, the contact angle of water on CTF-NH_2-F was measured at a reduced value of 51°, in contrast to that observed for CTF-NH_2 (75°) (Figure 2c,f). These findings suggest that the residual TfOH molecules interact with the pendant -NH_2 groups in the CTF framework, thereby enhancing the degree of hydrophilicity for CTF-NH_2-F.

Furthermore, the photoelectric properties of CTF-NH_2 and CTF-NH_2-F were measured and analyzed. The electrochemical impedance spectroscopy (EIS) curves can be accurately modeled using an equivalent circuit comprising a resistor (R)-constant phase capacitor (CPE) element. The Re and Rct parameters represent the electrolyte resistance and charge transfer resistance in samples, respectively [29,30]. These values are summarized in Table S2. The Rct value of CTF-NH_2-F is about 8.2 kΩ, which is remarkably smaller than that of CTF-NH_2 (Figure 4a); there was a slight improvement observed in the photocurrent of CTF-NH_2-F (Figure 4b), indicating the faster separation of photogenerated charge carriers in CTF-NH_2-F under an applied electric field. However, the photoluminescence intensity of CTF-NH_2-F was found to be higher than that of CTF-NH_2 (Figure 4c). Meanwhile, the fluorescent lifetime of CTF-NH_2-F was calculated to be 1.94 ns, which is shorter than that of CTF-NH_2

(Figure 4d), indicating a greater occurrence of radiative transitions of photogenerated charge carriers in CTF-NH_2-F. These findings are inconsistent with the photocatalytic performance of CTF-NH_2 and CTF-NH_2-F, distinguishing them from traditional photocatalysts.

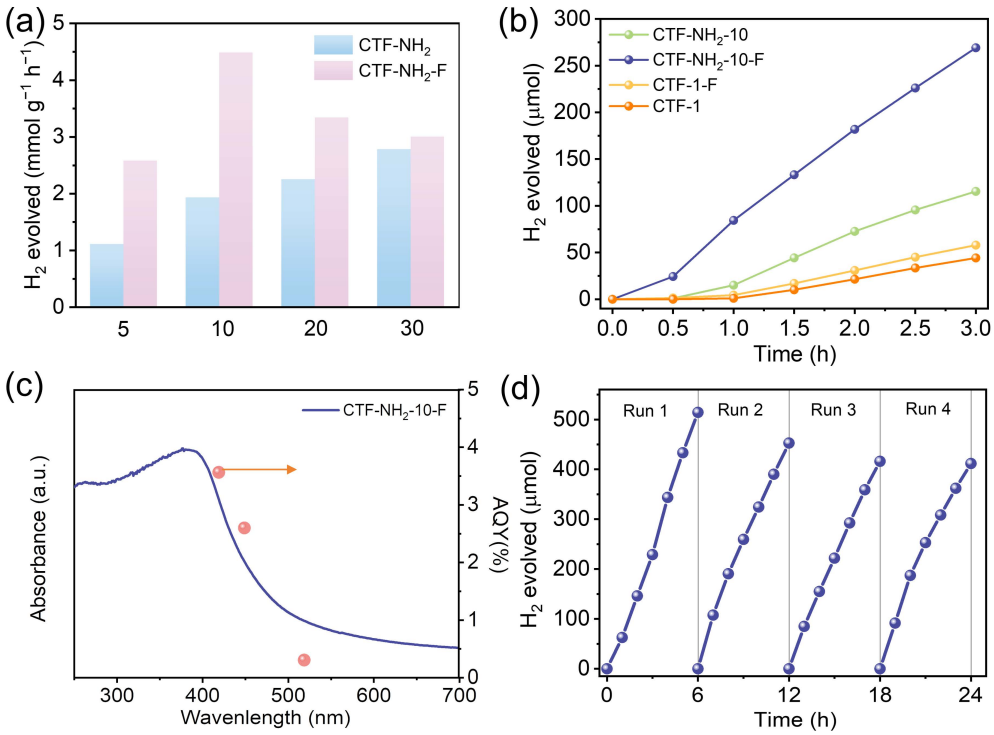

Figure 3. (**a**) H_2-evolving rates of CTF-NH_2 and CTF-NH_2-F (the values along the horizontal axis represent the mole ratio between dicyanobenzene and amino monomer), (**b**) photocatalytic H_2 evolution of CTF-NH_2-10, CTF-NH_2-10-F, CTF-1 and CTF-1-F, (**c**) wavelength-dependent AQY values (at 420 nm, 450 nm, 520 nm) and (**d**) photostability test of CTF-NH_2-10-F.

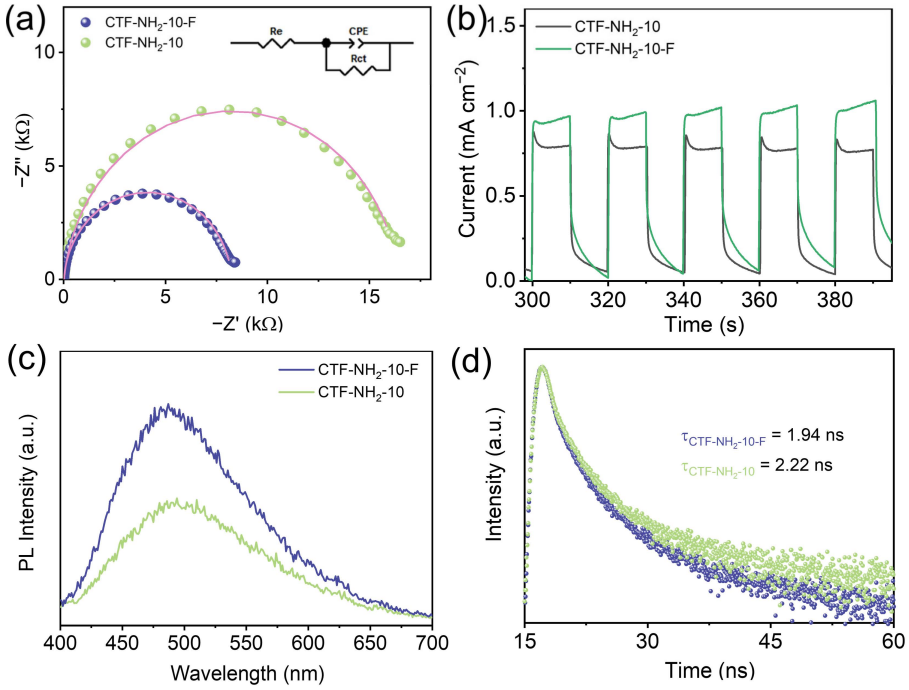

Figure 4. (**a**) EIS Nyquist plots, (**b**) photocurrent response curves, (**c**) steady-state PL spectra, (**d**) and time-resolved PL decay spectra of CTF-NH_2-10 and CTF-NH_2-10-F.

In light of the Pt cocatalyst employed in photocatalysis, we further conducted a comparative analysis of photoelectric properties of Pt-loaded photocatalysts. The XPS survey spectra and high-resolution Pt 4f spectra reveal the presence of elemental Pt (Figure S6a,b), demonstrating the successful loading of Pt onto the surfaces of CTF-NH_2 and CTF-NH_2-F [31,32]. The FT-IR spectra show no significant alterations in CTF-NH_2 with and without Pt loading (Figure S6c). In contrast, the stretching vibrations of -SO_3H exhibit a decrease in intensity after Pt loading (Figure S6d), indicating that residual TfOH may interact with the Pt nanoparticles [33,34]. In comparison to CTF-NH_2 and CTF-NH_2-F (Figure 4), the Pt-loaded photocatalysts CTF-NH_2/Pt and CTF-NH_2-F/Pt exhibited decreased radii in EIS, enhanced photocurrent density, diminished photoluminescence, and shortened fluorescent lifetime (Figure 5). In particularly, CTF-NH_2-F/Pt exhibited more obvious properties. Of note, the photoluminescence intensity of CTF-NH_2-F/Pt decreased to a much lower level compared to that of CTF-NH_2/Pt (Figure 5c). These results indicate that the loaded Pt nanoparticles lead to a pronounced reduction in radiative transfer by extracting photogenerated electrons from CTF-NH_2.

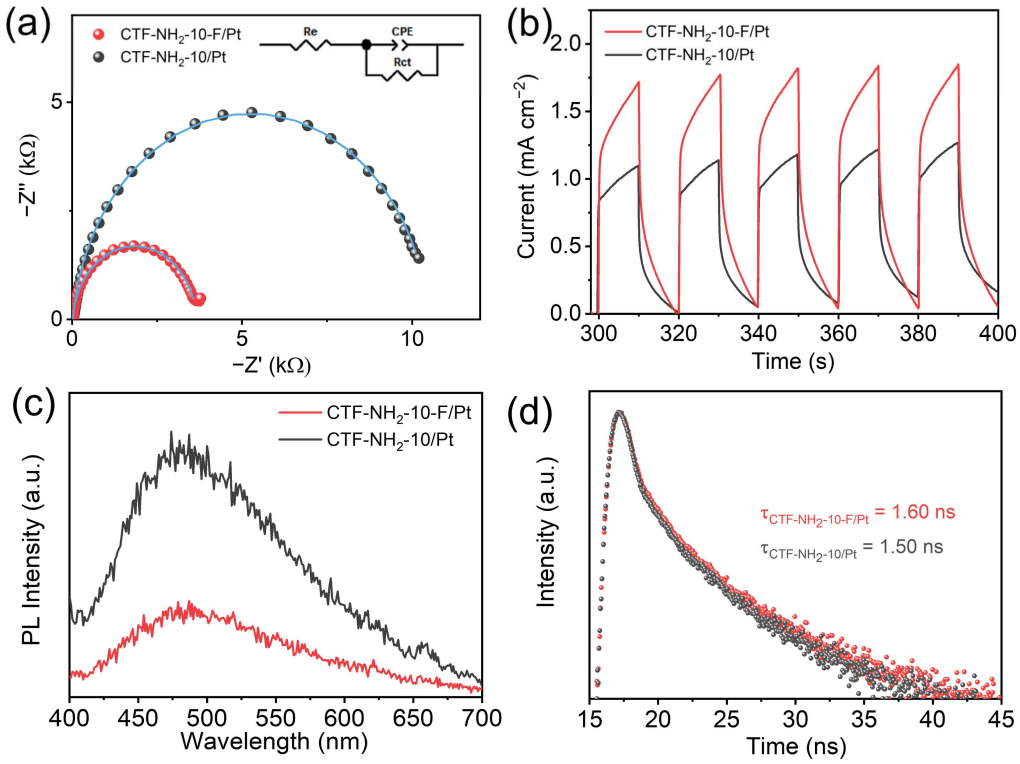

Figure 5. (**a**) EIS Nyquist plots, (**b**) photocurrent response curves, (**c**) steady-state PL spectra, and (**d**) time-resolved PL decay spectra of CTF-NH_2-10/Pt and CTF-NH_2-F-10/Pt.

Furthermore, the band structures of CTF-NH_2 and CTF-NH_2-F were confirmed by Tauc plots, XPS valence band spectra, and Mott–Schottky measurements. The UV–visible diffuse reflectance spectra revealed a slight blue shift in the absorption edge of CTF-NH_2-F, and correspondingly, the respective band gaps (E_g) of CTF-NH_2 and CTF-NH_2-F were determined as 2.64 eV and 2.76 eV based on their Tauc plots (Figure 6a,b). Furthermore, the conduction bands (E_{CB}) for CTF-NH_2 and CTF-NH_2-F were determined to be −1.25 V and −0.94 V (vs. Ag/AgCl), respectively, by analyzing the slopes of the Mott–Schottky plots, which are equivalent to energy levels of −0.99 eV and −0.64 eV (vs. RHE) (Figure 6c,d) [35]. The XPS-valence spectra unveiled the valence bands (E_{VB}) of 2.05 eV and 2.52 eV for CTF-NH_2 and CTF-NH_2-F, respectively, which were calibrated to the values of 1.65 eV and 2.12 eV (vs. RHE, pH = 0) (Figure 6e), due to the work function of the XPS analyzer being

ca. 4 eV (vs. vacuum) and −0.4 V (vs. RHE at pH = 0) [36–38]. These values demonstrate a strong correlation with the formula $E_g = E_{VB} - E_{CB}$. The aforementioned results suggest that residual TfOH has a marginal impact on visible light absorption while affecting the CB and VB positions. The more positive E_{VB} of CTF-NH_2-F reflects its enhanced ability to oxidize water and sacrificial agents (Figure 6f).

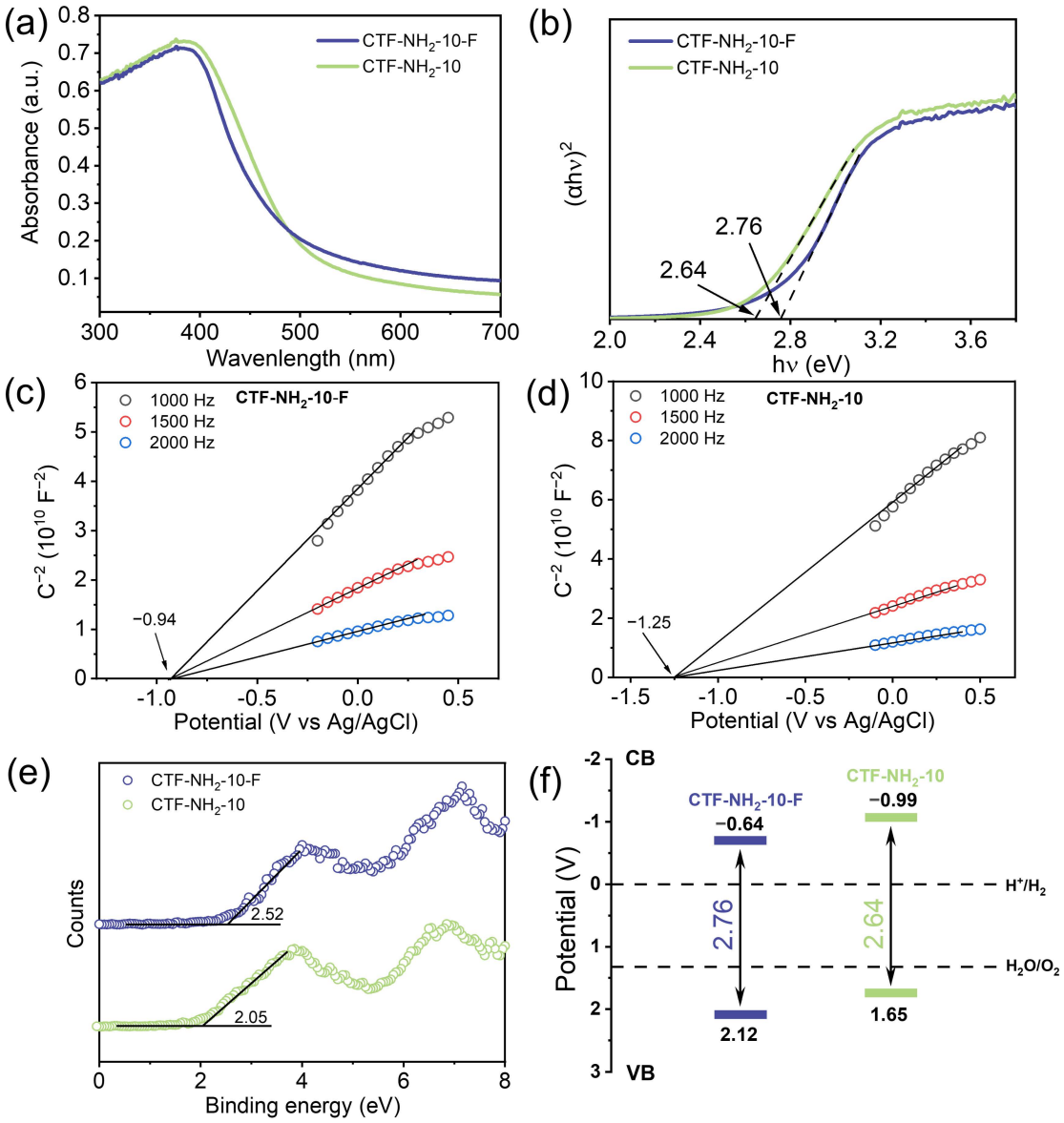

Figure 6. (**a**) UV–vis diffuse reflectance spectra, (**b**) Tauc plots, (**c**,**d**) Mott–Schottky plots, (**e**) XPS-valence spectra, and (**f**) band diagrams of CTF-NH_2-10 and CTF-NH_2-10-F.

3. Conclusions

The synthesis of CTF-NH_2 functionalized with amino groups was achieved through the catalysis of the organic strong acid TfOH. In the absence of ammonia treatment, some TfOH molecules were found to reside in the CTF-NH_2-F structure. The TfOH molecules primarily engage in hydrogen bonding interactions with the amino groups, allowing TfOH to remain within CTF-NH_2-F below 340 °C. The presence of residual TfOH in CTF-NH_2-F might induce significant radiation transition of photogenerated charge carriers; however, the utilization of Pt cocatalyst enabled a more efficient separation of photogenerated charge carriers within CTF-NH_2-F compared to that within CTF-NH_2. Moreover, the residual TfOH

increased the VB position of CTF-NH_2-F, facilitating water oxidization or consumption of photogenerated holes. The photocatalytic hydrogen evolution of CTF-NH_2-F could reach about 4.5 mmol g^{-1} h^{-1}, with an AQY of 3.56% at 420 nm, which is 2.5 times higher than that of CTF-NH_2.

Supplementary Materials: The following supporting information can be downloaded at: https://www.mdpi.com/article/10.3390/catal15010012/s1, Figure S1: The structures of CTF-NH_2 and CTF-NH_2-F; Figure S2: High-resolution C 1s and O 1s XPS spectra of CTF-NH_2-10 and CTF-NH_2-10-F; Figure S3: XRD spectra of CTF-NH_2-10-F and CTF-NH_2-10; Figure S4: Photocatalytic H_2 evolution of CTF-NH_2-x; Figure S5: Photocatalytic H_2 evolution of CTF-NH_2-F; Figure S6: XPS survey spectra, Pt high-resolution spectra, FT-IR spectra of CTF-NH_2-10/Pt and CTF-NH_2-10-F/Pt; Table S1: Elemental analysis date for CTF-NH_2-10-F; Table S2: EIS parameters obtained from the fitting of CTFs. References [28,35] are cited in the Supplementary information.

Author Contributions: Conceptualization, C.Z. and W.X.; methodology, C.Z., Z.L. and W.X.; validation, W.X.; data curation, Z.L.; writing—original draft preparation, C.Z., Z.L. and W.X.; writing—review and editing, C.Z.; supervision, W.X.; project administration, C.Z.; funding acquisition, C.Z. All authors have read and agreed to the published version of the manuscript.

Funding: This research was supported by grants from the National Natural Science Foundation of China (No. 22005149) and Natural Science Foundation of Jiangsu Province (No. BK20200777).

Data Availability Statement: All data are contained within this article or Supplementary Materials.

Conflicts of Interest: The authors declare no conflicts of interest.

References

1. Tao, X.; Zhao, Y.; Wang, S.; Li, C.; Li, R. Recent advances and perspectives for solar-driven water splitting using particulate photocatalysts. *Chem. Soc. Rev.* **2022**, *51*, 3561–3608. [CrossRef] [PubMed]
2. Hota, P.; Das, A.; Maiti, D.K. A short review on generation of green fuel hydrogen through water splitting. *Int. J. Hydrogen Energy* **2023**, *48*, 523–541. [CrossRef]
3. Yan, Z.; Yin, K.; Xu, M.; Fang, N.; Yu, W.; Chu, Y.; Shu, S. Photocatalysis for synergistic water remediation and H_2 production: A review. *Chem. Eng. J.* **2023**, *472*, 145066. [CrossRef]
4. Meng, J.Y.; Huang, Y.M.; Wang, X.L.; Liao, Y.F.; Zhang, H.H.; Dai, W.L. Photocatalytic Production of Hydrogen Peroxide from Covalent-Organic-Framework-Based Materials: A Mini-Review. *Catalysts* **2024**, *14*, 429. [CrossRef]
5. Li, Y.; Song, X.; Zhang, G.; Wang, L.; Liu, Y.; Chen, W.; Chen, L. 2D Covalent Organic Frameworks Toward Efficient Photocatalytic Hydrogen Evolution. *ChemSusChem* **2022**, *15*, e202200901. [CrossRef]
6. He, T.; Zhao, Y. Covalent Organic Frameworks for Energy Conversion in Photocatalysis. *Angew. Chem. Int. Ed.* **2023**, *62*, e202303086. [CrossRef]
7. Zhao, C.; Han, C.; Yang, X.; Xu, J. Synthesis of two-dimensional ultrathin photocatalytic materials towards a more sustainable environment. *Green Chem.* **2022**, *24*, 4728–4741. [CrossRef]
8. Chen, Z.; Wang, J.; Hao, M.; Xie, Y.; Liu, X.; Yang, H.; Waterhouse, G.I.N.; Wang, X.; Ma, S. Tuning excited state electronic structure and charge transport in covalent organic frameworks for enhanced photocatalytic performance. *Nat. Commun.* **2023**, *14*, 1106. [CrossRef]
9. López-Magano, A.; Daliran, S.; Oveisi, A.R.; Mas-Ballesté, R.; Dhakshinamoorthy, A.; Alemán, J.; Garcia, H.; Luque, R. Recent Advances in the Use of Covalent Organic Frameworks as Heterogenous Photocatalysts in Organic Synthesis. *Adv. Mater.* **2023**, *35*, 2209475. [CrossRef]
10. An, B.; Zheng, B.; Liu, Z.; Wu, Z.; Wu, M.; Wu, W. Covalent organic frameworks for photochemical organic synthesis. *Curr. Opin. Green Sustain. Chem.* **2023**, *41*, 100798. [CrossRef]
11. Chen, J.; Yuan, D.; Wang, Y. Covalent Organic Frameworks Based Heterostructure in Solar-To-Fuel Conversion. *Adv. Funct. Mater.* **2023**, *33*, 2304071. [CrossRef]
12. Rahman, T.U.; Roy, H.; Fariha, A.; Shoronika, A.Z.; Al-Mamun, M.R.; Islam, S.Z.; Islam, M.S.; Marwani, H.M.; Islam, A.; Alsukaibi, A.K.D.; et al. Progress in plasma doping semiconductor photocatalysts for efficient pollutant remediation and hydrogen generation. *Sep. Purif. Technol.* **2023**, *320*, 124141. [CrossRef]

13. Kao, J.-C.; Teng, T.-Y.; Lin, H.-W.; Tseng, F.-G.; Ting, L.-Y.; Bhalothia, D.; Chou, H.-H.; Lo, Y.-C.; Chou, J.-P.; Chen, T.-Y. Single Atom Ag Bonding Between PF3T Nanocluster and TiO_2 Leads the Ultra-Stable Visible-Light-Driven Photocatalytic H_2 Production. *Small* **2024**, *20*, 2403176. [CrossRef] [PubMed]
14. Fu, X.; Wang, J.; Huang, D.; Meng, S.; Zhang, Z.; Li, L.; Miao, T.; Chen, S. Trace Amount of SnO_2-Decorated $ZnSn(OH)_6$ as Highly Efficient Photocatalyst for Decomposition of Gaseous Benzene: Synthesis, Photocatalytic Activity, and the Unrevealed Synergistic Effect between $ZnSn(OH)_6$ and SnO_2. *ACS Catal.* **2016**, *6*, 957–968. [CrossRef]
15. Bhalothia, D.; Wang, Z.-X.; Ting, L.-Y.; Chuang, Y.-T.; Chou, J.-P.; Lin, H.-W.; Tseng, F.-G.; Chou, H.-H.; Chen, T.-Y. Electron Coupling between the Linear-Conjugated Polymer Nanocluster and TiO_2 Nanoparticle Enables a Quantum Leap for Visible Light-Driven Hydrogen Evolution. *J. Phys. Chem. C* **2022**, *126*, 18596–18604. [CrossRef]
16. Huang, Y.H.; Wang, M.; Liu, W.; Wu, Q.; Hu, P. Unraveling the Prominent Existence of Trace Metals in Photocatalysis: Exploring Iron Impurity Effects. *J. Org. Chem.* **2024**, *89*, 4156–4164. [CrossRef]
17. Wu, M.Y.; Wu, Z.G.; Ang, H.T.; Wang, B.; Liu, T.; Wu, S.F.; Lei, Z.X.; Liaw, M.W.; Chanmungkalakul, S.; Lee, C.L.K.; et al. Enhanced Reactivity of Acridinium Perchlorate: Harnessing Redox Mediators for Trace Chloride Activation in Hydrogen Atom Transfer Photocatalysis. *ACS Catal.* **2024**, *14*, 9364–9373. [CrossRef]
18. Qian, Z.; Wang, Z.J.; Zhang, K.A.I. Covalent Triazine Frameworks as Emerging Heterogeneous Photocatalysts. *Chem. Mater.* **2021**, *33*, 1909–1926. [CrossRef]
19. Guo, L.; Wang, X.; Zhan, Z.; Zhao, Y.; Chen, L.; Liu, T.; Tan, B.; Jin, S. Crystallization of Covalent Triazine Frameworks via a Heterogeneous Nucleation Approach for Efficient Photocatalytic Applications. *Chem. Mater.* **2021**, *33*, 1994–2003. [CrossRef]
20. Sun, R.; Tan, B. Covalent Triazine Frameworks (CTFs) for Photocatalytic Applications. *Chem. Res. Chin. Univ.* **2022**, *38*, 310–324. [CrossRef]
21. Li, Z.; Fang, H.; Chen, Z.; Zou, W.; Zhao, C.; Yang, X. Regulating donor-acceptor interactions in triazine-based conjugated polymers for boosted photocatalytic hydrogen production. *Appl. Catal. B Environ.* **2022**, *312*, 121374. [CrossRef]
22. Zhu, Y.; Chen, X.; Cao, Y.; Peng, W.; Li, Y.; Zhang, G.; Zhang, F.; Fan, X. Reversible intercalation and exfoliation of layered covalent triazine frameworks for enhanced lithium ion storage. *Chem. Commun.* **2019**, *55*, 1434–1437. [CrossRef] [PubMed]
23. Zhao, C.; Li, Z.; Wu, X.; Su, H.; Bai, F.-q.; Ran, X.; Yang, L.; Fang, W.; Yang, X. Theory-Guided Experimental Design of Covalent Triazine Frameworks for Efficient Photocatalytic Hydrogen Production. *Small* **2024**, *20*, 2400541. [CrossRef] [PubMed]
24. Li, Z.; Li, T.; Miao, J.; Zhao, C.; Jing, Y.; Han, F.; Zhang, K.; Yang, X. Amide-functionalized covalent triazine framework for enhanced photocatalytic hydrogen evolution. *Sci. China Mater.* **2023**, *66*, 2290–2298. [CrossRef]
25. Yang, Z.; Chen, H.; Wang, S.; Guo, W.; Wang, T.; Suo, X.; Jiang, D.-e.; Zhu, X.; Popovs, I.; Dai, S. Transformation Strategy for Highly Crystalline Covalent Triazine Frameworks: From Staggered AB to Eclipsed AA Stacking. *J. Am. Chem. Soc.* **2020**, *142*, 6856–6860. [CrossRef]
26. Huang, W.; Li, B.; Wu, Y.; Zhang, Y.; Zhang, W.; Chen, S.; Fu, Y.; Yan, T.; Ma, H. In Situ-Doped Superacid in the Covalent Triazine Framework Membrane for Anhydrous Proton Conduction in a Wide Temperature Range from Subzero to Elevated Temperature. *ACS Appl. Mater. Interfaces* **2021**, *13*, 13604–13612. [CrossRef]
27. Li, Y.; Zhang, R.; Li, C.; Li, H.; Fang, Q.; Xie, T. Fabrication of electron–acceptor staggered AB Covalent triazine-based frameworks for enhanced visible-light-driven H_2 evolution. *J. Colloid Interface Sci.* **2022**, *608*, 1449–1456. [CrossRef]
28. Ran, J.; Gao, G.; Li, F.T.; Ma, T.Y.; Du, A.; Qiao, S.Z. Ti_3C_2 MXene co-catalyst on metal sulfide photo-absorbers for enhanced visible-light photocatalytic hydrogen production. *Nat. Commun.* **2017**, *8*, 13907. [CrossRef]
29. Li, J.; Liu, X.; Sun, Z.; Sun, Y.; Pan, L. Novel yolk–shell structure bismuth-rich bismuth molybdate microspheres for enhanced visible light photocatalysis. *J. Colloid Interf. Sci.* **2015**, *452*, 109–115. [CrossRef]
30. Liu, C.; Busse, S.; Liu, J.; Godin, R. Aminosilanized Interface Promotes Electrochemically Stable Carbon Nitride Films with Fewer Trap States on FTO for (Photo)electrochemical Systems. *ACS Appl. Mater. Interfaces* **2023**, *15*, 46902–46915. [CrossRef]
31. Gao, H.; Neale, A.R.; Zhu, Q.; Bahri, M.; Wang, X.; Yang, H.; Xu, Y.; Clowes, R.; Browning, N.D.; Little, M.A.; et al. A Pyrene-4,5,9,10-Tetraone-Based Covalent Organic Framework Delivers High Specific Capacity as a Li-Ion Positive Electrode. *J. Am. Chem. Soc.* **2022**, *144*, 9434–9442. [CrossRef] [PubMed]
32. Zhao, Z.; Chen, W.; Zhang, G.; Chen, Y. Interface molecular wires induce electron transfer from COFs to Pt for enhanced photocatalytic H2 evolution. *J. Mater. Chem. A* **2023**, *11*, 26052–26062. [CrossRef]
33. Furuya, Y.; Mashio, T.; Ohma, A.; Dale, N.; Oshihara, K.; Jerkiewicz, G. Surface oxide growth on platinum electrode in aqueous trifluoromethanesulfonic acid. *J. Chem. Phys.* **2014**, *141*, 164705. [CrossRef]
34. Tang, M.; Yan, H.; Zhang, X.; Zheng, Z.; Chen, S. Materials Strategies Tackling Interfacial Issues in Catalyst Layers of Proton Exchange Membrane Fuel Cells. *Adv. Mater.* **2023**, 2306387. [CrossRef]
35. Zhang, T.; Hou, Y.; Dzhagan, V.; Liao, Z.Q.; Chai, G.L.; Loffler, M.; Olianas, D.; Milani, A.; Xu, S.Q.; Tommasini, M.; et al. Copper-surface-mediated synthesis of acetylenic carbon-rich nanofibers for active metal-free photocathodes. *Nat. Commun.* **2018**, *9*, 1140. [CrossRef]

36. Greczynski, G.; Hultman, L. X-ray photoelectron spectroscopy: Towards reliable binding energy referencing. *Prog. Mater Sci.* **2020**, *107*, 100591. [CrossRef]
37. Li, L.; Zhu, Y.; Gong, N.; Zhang, W.; Peng, W.; Li, Y.; Zhang, F.; Fan, X. Band-gap engineering of layered covalent organic frameworks via controllable exfoliation for enhanced visible-light-driven hydrogen evolution. *Int. J. Hydrogen Energy* **2020**, *45*, 2689–2698. [CrossRef]
38. Kong, D.; Han, X.; Xie, J.; Ruan, Q.; Windle, C.D.; Gadipelli, S.; Shen, K.; Bai, Z.; Guo, Z.; Tang, J. Tunable covalent triazine-based frame works (CTF-0) for visible-light-driven hydrogen and oxygen generation from water splitting. *ACS Catal.* **2019**, *9*, 7697–7707. [CrossRef]